Ultrasonics Sonochemistry 90 (2022) 106214

Contents lists available at ScienceDirect

Ultrasonics Sonochemistry

journal homepage: www.elsevier.com/locate/ultson

Effects of gas saturation and sparging on sonochemical oxidation activity in open and closed systems, Part I: H_2O_2 generation

Younggyu Son [a,b,*], Jieun Seo [a,c]

[a] Department of Environmental Engineering, Kumoh National Institute of Technology, Gumi 39177, Republic of Korea
[b] Department of Energy Engineering Convergence, Kumoh National Institute of Technology, Gumi 39177, Republic of Korea
[c] Environment Research Division, Gyeongsangbuk-do Government Public Institute of Health & Environment, Yeongcheon 38874, Republic of Korea

ARTICLE INFO

Keywords:
Acoustic cavitation
Gas saturation
Gas sparging
H_2O_2 generation
Sonochemiluminescence
Dissolved oxygen

ABSTRACT

Cavitational/sonochemical activity can be significantly enhanced or reduced depending on the gases dissolved in the liquid. Although many researchers have suggested the order of importance of dissolved gas conditions that affect the degree of sonoluminescence (SL), sonochemiluminescence (SCL), and compound degradation, the most suitable gas condition for sonochemical oxidation reactions is currently unknown. In this study (Part I), the effects of gas saturation and sparging on the generation of H_2O_2 were investigated in a 28-kHz sonoreactor system. Four gas modes, saturation/closed, saturation/open, sparging/closed, and sparging/open, were applied to Ar, O_2, N_2, and binary gas mixtures. The change in dissolved oxygen (DO) concentration during ultrasonic irradiation was measured and was used as an indicator of whether the gaseous exchange between liquid and air altered the gas content of the liquid. Considerable difference in the DO concentration was observed for the gas saturation/open mode, ranging from –11.5 mg/L (O_2 100 %) to +4.3 mg/L (N_2 100 %), while no significant difference was observed in the other gas modes. The change in the gas content significantly reduced the linearity for H_2O_2 generation, which followed pseudo-zero-order kinetics, and either positively or negatively affected H_2O_2 generation. Ar:O_2 (75:25) and Ar:O_2 (50:50) resulted in the highest and second-highest H_2O_2 generation for both gas saturation and sparging, respectively. In addition, gas sparging resulted in much higher H_2O_2 generation for all gas conditions compared to gas saturation; this was because of the significant change in the cavitational active zone and concentrated ultrasonic energy, which formed a bulb-shaped active zone, especially for the Ar/O_2 mixtures adjacent to the transducer at the bottom. The sparging flow rate and position also significantly affected H_2O_2 generation; the highest H_2O_2 generation was obtained when the sparger was placed at the bottom adjacent to the transducer, with a flow rate of 3 L/min.

In Part II, the generation of nitrogen oxides, including nitrite (NO_2^-) and nitrate (NO_3^-), was investigated using the same ultrasonic system with three gas modes: saturation/open, saturation/closed, and sparging/closed.

1. Introduction

The effects of dissolved gases on cavitational and sonochemical activity have been widely investigated using N_2, O_2, Ar, and CO_2 under single gas or gas mixture conditions, including air [1–5]. Sonoluminescence (SL), sonochemiluminescence (SCL), and sonochemical oxidation/reduction activity (KI dosimetry, H_2O_2 generation, and aqueous pollutant degradation) have been studied under various frequency conditions in sonochemistry. A few researchers have also tested the effects of rare/noble gases, including H_2, He, Ne, Ar, Kr, and Xe [1,2,6,7].

Previous researchers have reported that a much higher sonochemical oxidation activity can be obtained with the use of a mixture of Ar and O_2 as the saturation gases, in comparison to the individual use of Ar, O_2, and air. A combination of Ar with O_2 in the range of 20–30 % is generally considered to be the best mixture condition for the highest sonochemical oxidation activity [2,8,9]. Rooze et al. compared the reaction kinetic constants for Ar and air using the results of previous studies, and reported that the suitable saturation gas differed depending on the frequency and target reaction [1]. They suggested that Ar was more suitable in 20 kHz systems than in systems with higher frequencies for KI oxidation and was more effective for the degradation of chlorinated

Abbreviations: SL, sonoluminescence; SCL, sonochemiluminescence; DO, dissolved oxygen.

* Corresponding author at: Department of Environmental Engineering, Kumoh National Institute of Technology, Gumi 39177, Republic of Korea.
E-mail address: yson@kumoh.ac.kr (Y. Son).

https://doi.org/10.1016/j.ultsonch.2022.106214
Received 26 August 2022; Received in revised form 10 October 2022; Accepted 27 October 2022
Available online 28 October 2022

compounds than for non-chlorinated compounds. Merouani et al. simulated the sonochemical OH radical generation rate for Ar, O_2, air, and N_2 and found that the order of generation was O_2 > air > N_2 > Ar at frequencies ranging from 213 to 355 kHz, while the order was Ar > O_2 > air > N_2 at 515 kHz and higher [10]. They also summarized the order of dissolved gases for the degradation of organic compounds and generation of H_2O_2 in the frequency range of 200–1140 kHz using the experimental results from previous research, and found that their simulated gas orders were quite similar to those in previous studies.

While frequency is considered one of the most important factors for determining the optimal gas conditions for sonochemical oxidation activity, the degree of gas saturation during ultrasonic irradiation should also be considered to appropriately compare the sonochemical activity under various saturation gas conditions. This is because the amount and composition of dissolved gases can change significantly via gas exchange phenomena, induced by the gas concentration gradient across the air–water interface. Ultrasonic degassing also plays an important role in the removal of gas molecules [11–13]. However, the concentrations of dissolved gases have rarely been monitored, and few researchers have reported the concentrations of dissolved oxygen (DO) before and after ultrasonic irradiation [12,14–16]. In some studies, researchers continuously supplied gases throughout ultrasonic irradiation, using a sparger, to maintain the gas content in the liquid phase [4,5,14,17–20]. However, the application of gas sparging can significantly alter the formation of the sound energy field and cavitational active zone in comparison to gas saturation conditions because of the generation and movement of large gas bubbles [4,5,14,19,21]. Therefore, whether the system is open to air, how many gas molecules are removed via ultrasonic degassing, and whether sparging is applied under various gas conditions is vital to holistically investigate the effect of dissolved gases on sonochemical oxidation activity.

Recently, there has been growing interest in the on-site generation of H_2O_2 using various methods to reduce the risk and cost of H_2O_2 storage, transportation, and use [22,23]. Sonochemical methods have proven effective for the generation of H_2O_2 for decades [7,14,15,24–28]. Even though higher generation rate of H_2O_2 could be obtained in the range of several hundred kilohertz [2], it was reported that low frequency (20 – 40 kHz) ultrasound could be more appropriate for large-scale sonoreactors [28–31]. In this study (Part I), four modes of gas saturation/sparging, including saturation/closed, saturation/open, sparging/closed, and sparging/open, were investigated to understand the effect of dissolved gases on the generation of H_2O_2, representing the sonochemical oxidation activity, using Ar, O_2, N_2, and their binary mixtures in a 28-kHz sonoreactor system. The DO concentration was measured before and after ultrasonic irradiation to estimate the change in gas content in the liquid. SCL images for all cases were obtained to understand the variation in the cavitational active zones and the resulting sonochemical oxidation activity. In the companion paper (Part II), the effect of dissolved gases on the generation of nitrogen oxides, including nitrite (NO_2^-) and nitrate (NO_3^-) is discussed under the same gas saturation and sparging conditions.

2. Experimental methods

2.1. Chemicals

Hydrogen peroxide (H_2O_2) and sodium hydroxide (NaOH) were obtained from Samchun Pure Chemical Co. ltd. (KOR). Potassium biphthalate (C_8H_5KO4) was acquired from Daejung Chemical &Metals Co. ltd. (KOR). Potassium iodide (KI) and ammonium molybdate [$(NH_4)_2MoO_4$] were purchased from Junsei Chemical Co. ltd. (JPN). Luminol (3-aminophthalhydrazide, $C_8H_7N_3O_2$) was acquired from Sigma–Aldrich Co. (USA). All chemicals were used as received.

2.2. Sonoreactor and gas supply

An acrylic cylindrical sonoreactor was used in this study, equipped with a 28 kHz transducer module (Mirae Ultrasonic Tech., Bucheon, KOR) that was placed at the bottom as shown in Fig. 1. The inner diameter and height of the sonoreactor was 150 mm and 350 mm, respectively. The liquid height was determined using the following equation:

$$\lambda = \frac{c}{f} \tag{1}$$

where λ is the wavelength, c is the speed of sound in water (1500 m/s), and f is the applied frequency (28 kHz). The liquid height and volume were 4.0 λ (53.6 mm) and 3.65 L, respectively [4,32,33]. The temperature in the liquid body was maintained at 20 ℃ using a cooling system consisting of a cooling pipe attached to the side wall of the reactor and a water chiller. The working electrical power was 100 W, measured using a power meter (HPM-300A; ADpower, KOR), and the ultrasonic power, or calorimetric power, was 55 W [34–36].

As shown in the inset of Fig. 1, four modes of gas saturation and sparging were examined using a gas supply system including gas cylinders of Ar, O_2, and N_2, mass flow controllers (HFC-D-302B; Teledyne Hastings Instruments, USA), a static mixer (Gasline, Seongnam, KOR), a mass flow meter (HFM-D-300B; Teledyne Hastings Instruments, USA), and a gas flow monitoring controller. The modes were: 1) Saturation/closed mode, wherein the liquid was saturated with a gas or gas mixture and the top of the reactor was covered with a sealing lid (the gas content in the headspace was considered to be the same as the gas content in the liquid body). 2) Saturation/open mode, wherein the liquid was saturated with a gas or gas mixture, and the liquid body was open to air without a sealing lid (the gas content change in the liquid body occurred owing to the interaction with air). 3) Sparging/closed mode, wherein a gas or gas mixture was supplied continuously to the liquid body after saturation was reached, and the gas outlet in the sealing lid was slightly open to prevent an increase in gas pressure due to the continuous gas supply (no gas intrusion occurred). 4) Sparging/open mode, which was open to air, a gas or gas mixture was supplied continuously to the liquid body after saturation was reached (gaseous exchange between liquid and air could occur). Twelve types of pure gases and gas mixtures were used in this study, including Ar, Ar:O_2 (75:25), Ar:O_2 (50:50), Ar:O_2 (25:75), O_2, O_2:N_2 (75:25), O_2:N_2 (50:50), O_2:N_2 (25:75), N_2, N_2:Ar (75:25), N_2:Ar (50:50), and N_2:Ar (25:75). Gas was delivered into the liquid body using a microporous glass sparger (pore size: 20–30 μm) equipped with a glass pipe. The sparger was placed 1 cm above the reactor bottom [4]. The gas flow rate for saturation and sparging was 3 L/min. The DO concentration was measured before and after each test using a DO meter to estimate the degree of gas saturation in the liquid body (ProODO; YSI Inc., USA).

2.3. Quantification of sonochemical reactions

The concentration of sonochemically generated H_2O_2 was spectrophotometrically analyzed using solution A (0.10 M potassium biphthalate), solution B (0.4 M KI, 0.06 M sodium hydroxide, and 10^{-4} M ammonium molybdate), and a UV–vis spectrophotometer (SPECORD 40; Analytic Jena AG, Jena, DEU) [28,35].

2.4. Visualization of sonochemical reactions

The sonochemically active zone was visualized using luminol solution (0.1 g/L luminol and 1 g/L NaOH) in a completely dark room [36–38]. Sonochemiluminescence images were acquired using an exposure-controlled digital camera (α58; Sony Corp., JPN) with an exposure time of 30 s.

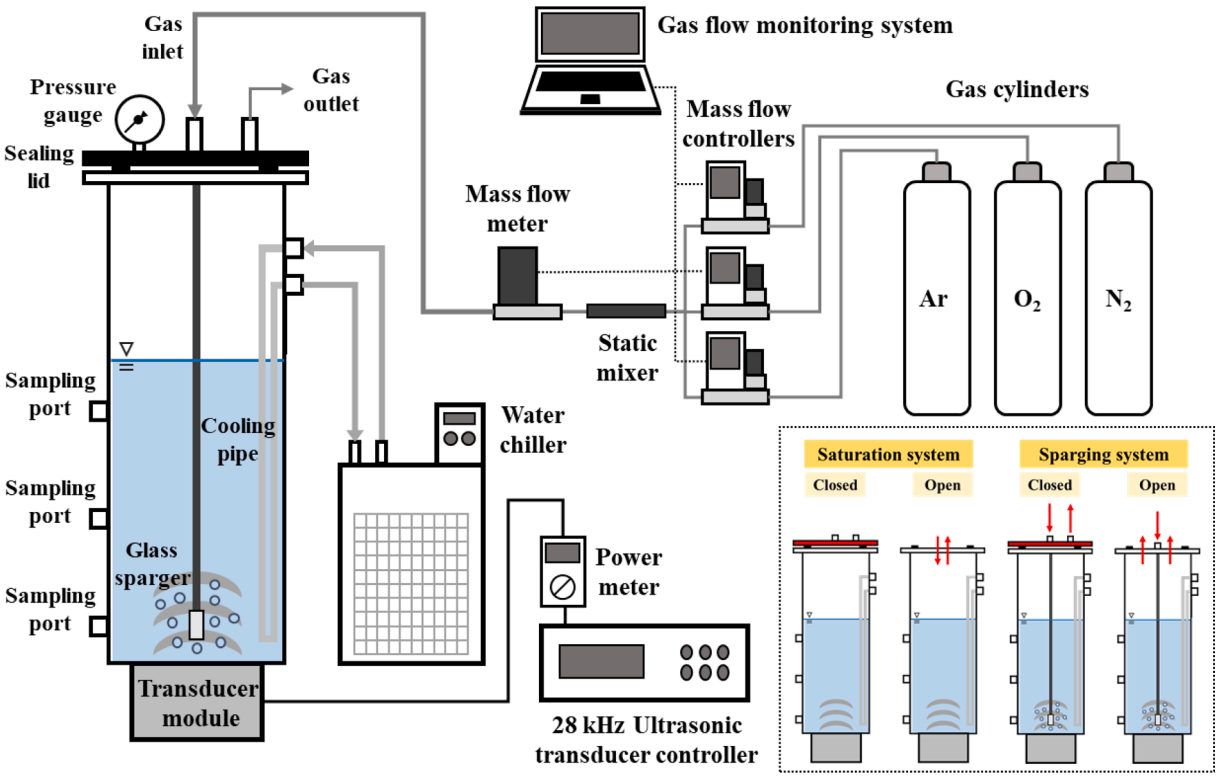

Fig. 1. Schematic of the sonoreactor with the gas supply system. The inset represents the four modes of gas saturation/sparging used in this study. In the open modes, gaseous exchange between liquid and air could occur. In the gas sparging/closed mode, the outlet in the sealing lid was slightly open to prevent an increase in gas pressure due to the continuous gas supply (no gas intrusion occurred).

2.5. Analysis of acoustic emission spectra

The sound pressure levels for the fundamental frequency (f), harmonic frequencies (2f, 3f, 4f, •••), and subharmonic frequencies (1.5f, 2.5f, 3.5f, •••) were monitored from 0 to 500 kHz using a hydrophone (TC4034, Reson) and spectrum analyzer (N9320B, Keysight). The hydrophone was placed in the middle of the reactor, and the sparger at the bottom. The sound pressure level, measured in voltage (V), was recorded for 5 s.

3. Results and discussion

3.1. Gas saturation

During ultrasonic irradiation, acoustic cavitation events occur continuously, and cavitation-induced oxidizing radicals such as OH radicals are generated and consumed to generate H_2O_2, as shown in the following reactions [39,40]:

$$\cdot OH + \cdot OH \rightleftharpoons H_2O_2 \quad (2)$$

$$H_2O + \cdot OH \rightleftharpoons H_2O_2 + \cdot H \quad (3)$$

$$HO_2\cdot + HO_2\cdot \rightleftharpoons H_2O_2 + O_2 \quad (4)$$

$$HO_2\cdot + H_2 \rightleftharpoons H_2O_2 + H\cdot \quad (5)$$

$$HO_2\cdot + \cdot OH \rightleftharpoons H_2O_2 + O \quad (6)$$

$$HO_2\cdot + H_2O \rightleftharpoons H_2O_2 + \cdot OH \quad (7)$$

$$\cdot OH + H_2O + O_2 \rightleftharpoons H_2O_2 + HO_2\cdot \quad (8)$$

Although the generated H_2O_2 molecules are consumed again in radical chain reactions, H_2O_2 molecules can accumulate linearly owing to the continuous generation of oxidizing radicals [28,41,42]. The generation of H_2O_2 can be maintained for several hours [43]. Therefore, the rate or amount of H_2O_2 generation has been used as an intuitive indicator of the extent of sonochemical oxidation reactions.

Fig. 2 shows the pseudo-zero-order reaction constant and its coefficient of determination for the sonochemical generation of H_2O_2 under various gas saturation conditions in closed and open systems. The irradiation duration was 60 min. The variations in the DO concentration before and after ultrasonic irradiation are summarized in Table 1. No significant change in the composition of the saturated gases was assumed during ultrasonic irradiation for all closed cases in this study, because only a relatively small change in the DO concentration was detected.

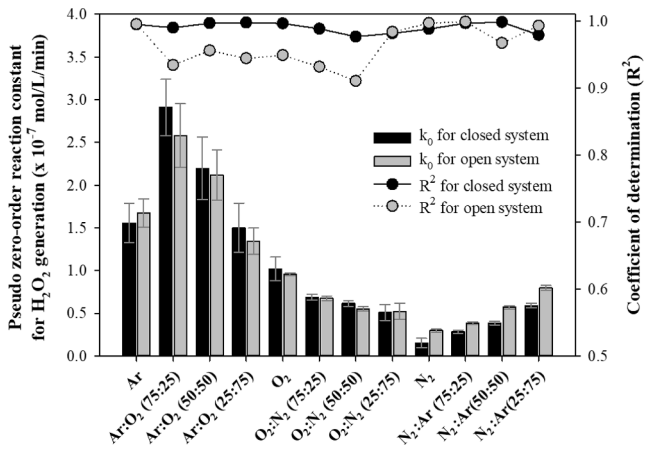

Fig. 2. Pseudo zero-order reaction constant and coefficient of determination for the 28 kHz cavitational generation of H_2O_2 under various gas saturation conditions in closed and open systems. The irradiation duration was 60 min.

Table 1
Variation of DO concentration before and after ultrasonic irradiation for various gas saturation conditions, with a DO saturation concentration of 9.1 mg/L at 20 ℃.

Gas saturation		Ar	Ar:O_2 (75:25)	Ar:O_2 (50:50)	Ar:O_2 (25:75)	O_2	O_2:N_2 (75:25)	O_2:N_2 (50:50)	O_2:N_2 (25:75)	N_2	N_2:Ar (75:25)	N_2:Ar (50:50)	N_2:Ar (25:75)
Closed	DO_0* (mg/L)	0.3	10.7	20.3	29.2	39.6	32.2	21.8	11.1	0.3	0.3	0.3	0.2
	DO_{60}* (mg/L)	0.7	10.3	20.0	28.7	38.4	31.5	21.5	11.2	0.8	0.8	0.9	0.8
	ΔDO**	+0.4	−0.4	−0.4	−0.5	−1.2	−0.8	−0.3	+0.0	+0.5	+0.4	+0.6	+0.5
Open	DO_0 (mg/L)	0.2	10.7	20.8	30.3	39.7	30.3	22.9	10.7	0.4	0.3	0.3	0.3
	DO_{60} (mg/L)	2.8	9.7	16.5	22.0	28.2	20.7	14.9	10.1	4.7	4.1	3.8	4.1
	ΔDO	+2.6	−1.0	−4.3	−8.4	−11.5	−9.6	−8.0	−0.6	+4.3	+3.9	+3.5	+3.9

* DO_0 and DO_{60} represent DO concentrations before and after 60 min of irradiation, respectively.
** $\Delta DO = DO_{60}\text{-}DO_0$.

In the closed system (water was saturated with a gas or gas mixture, and then the reactor was sealed during ultrasonic irradiation), higher reaction constants were obtained for the gas mixtures with Ar and O_2 [2,8,9,14,17,26,44]. The highest reaction constant was obtained for Ar:O_2 (75:25), 5.7 times higher than that for N_2:O_2 (75:25), which was similar to the air composition. Gas conditions with N_2 resulted in lower production. The lowest constant was obtained for N_2 [18,44–47], 3.3 times lower than that for N_2:O_2 (75:25). As the N_2 content increased under O_2:N_2 and N_2:Ar conditions, the reaction constant decreased drastically [48,49]. Therefore, Ar and O_2 played a positive role in the sonochemical generation of H_2O_2, while N_2 had a negative effect.

The physicochemical properties of Ar, O_2, and N_2 are summarized in Table 2. Monatomic gases such as Ar have higher values than do polyatomic gases such as O_2 and N_2, and a higher ratio of specific heat capacity results in extreme conditions inside the bubble, inducing greater cavitational activity [10]. The solubility of dissolved gas can be related to the number of cavitation nucleation events [1,50] and the dissolved gas molecules can grow and form larger bubbles, which become cavitationally active [51]. Cavitational bubbles containing dissolved gas molecules with lower thermal conductivity can maintain a larger concentrated energy inside the bubbles, causing more violent cavitation events [1,10,50]. The density and diffusivity of the dissolved gas can also be considered as secondary factors affecting the bubble growth mechanisms, including rectified diffusion and coalescence in cavitation events [52].

Even though a very high Ar content can positively affect the creation and maintenance of extreme conditions inside the bubble, the generated oxidizing radicals can be consumed because of the very high temperature [10]. It was reported that the generation of oxidizing radical species and H_2O_2 can be significantly enhanced in the presence of O_2, even though O_2 molecules do not act as a better source for oxidizing radicals than water molecules [8,9,14]. In addition, O_2 molecules act as scavengers for H radicals, which can consume oxidizing radicals such as OH radicals [1,46]. Beckett and Hua reported the lowest activity of oxidizing radical species for Ar at 100 % [8]. Pétrier et al. reported that the removal of 4-chlorophenol, a less volatile compound highly likely to undergo radical reactions outside the bubble, was faster for O_2 100 % than for Ar 100 % [54]. The presence of N_2 involves the formation of various nitrogen oxides, which results in smaller amounts of oxidizing radicals participating in the target oxidation reactions, including the generation of H_2O_2 [10,48,49]. It has also been reported that a higher tensile strength of water can be obtained for N_2 than for O_2 under the same gas dissolution concentration, which could undermine the number of cavitation events and the cavitational activity [55].

Table 2
Physico-chemical properties of Ar, O_2, and N_2 under 1 atm at 298–300 K [53].

Physico-chemical properties	Ar	O_2	N_2
Molecular weight ($g \bullet mol^{-1}$)	39.95	32.00	28.01
Density ($kg \bullet m^{-3}$)	1.603	1.284	1.123
Ratio of specific heat capacity (C_p/C_v)	1.67	1.40	1.40
Solubility in water (10^{-6} $mol \bullet m^{-3}$)	1.40	1.27	0.66
Thermal conductivity (10^{-3} $m \cdot kg \cdot s^{-3} \cdot K^{-1}$)	17.7	26.5	26.0
Diffusivity in water (10^{-9} $m^2 \bullet s^{-1}$)	2.5	2.42	2.0
Henry's law constant (10^{-6} $mol \bullet m^{-3} \bullet atm^{-1}$)	1.4	1.3	0.61
Composition in air (mole fraction, %)	0.9340	20.95	78.08

Therefore, a mixture of Ar and O_2 with a higher Ar content is essential to maximize the oxidizing radical activity. However, the presence of N_2 is detrimental to cavitational activity and markedly reduces the oxidizing radical activity due to the formation of nitrogen oxides.

In the open system (where water was saturated with a gas or gas mixture, before the water body was opened to air for the ultrasonic irradiation process), a trend very similar to that of the closed system was observed for the reaction constants under various gas conditions. However, relatively large differences in DO concentration before and after 60 min of ultrasonic irradiation were detected, as shown in Table 1. In this study, the concentrations of dissolved Ar and N_2 were not measured, and the change in DO concentration was considered as evidence of gaseous exchange across the air–water interface for O_2, Ar, and N_2. It is well known that absorption (dissolution) or desorption (degasification) of gases occurs when water is undersaturated or supersaturated [13]. Gaseous exchange between water and air can be significantly enhanced under turbulent conditions [11] and ultrasonic irradiation can cause mixing of the liquid body and gentle ripples at the liquid surface [4]. Moreover, ultrasonic degassing can affect the absorption/desorption of gases in liquids [56]. In this study, small bubbles formed, moved up, and escaped from the water surface.

Considerably higher reaction constants were obtained for the Ar 100 %, N_2 100 %, and Ar/N_2 mixture conditions in the open system compared to those in the closed system, as shown in Fig. 2. This was mainly attributed to the transfer of gases with a positive effect, such as O_2, from the atmosphere into the liquid. The DO concentration increased in the range of 2.6–4.3 mg/L for Ar 100 %, N_2 100 %, and Ar/N_2 mixture conditions, while the DO concentration decreased significantly (–1.0 to –11.5 mg/L) for other gas conditions. Ar is a rare gas in air, and consequently the removal of Ar from the liquid might occur much faster than that of O_2 and N_2. At 25 ℃, the air equilibrium concentrations of Ar, O_2, and N_2 were calculated as 0.013×10^{-3}, 0.272×10^{-3}, and 0.476×10^{-3} mol/L, respectively, and the solubilities were 107 times, 4.7 times, and 1.4 times higher than the equilibrium concentrations for Ar, O_2, and N_2, respectively. However, considering the enhancement of the reaction constant for Ar 100 % compared to that under the saturation/closed system, the addition of a smaller amount of O_2 via gaseous exchange seemed to be more advantageous than the removal of a larger amount of Ar during the 60 min irradiation duration in this study.

In contrast, lower reaction constants for the Ar/O_2 mixture, O_2 100 %, and O_2/N_2 mixture [O_2:N_2 (75:25) and O_2:N_2 (50:50)] conditions were obtained in the open system compared to those in the closed system. This was also attributed to the gas exchange between positively

affecting Ar and O_2 in the liquid and negatively affecting N_2 in the air, as indicated by the DO change in Table 1. No significant difference was observed for O_2:N_2 (25:75), because the gas composition was very similar to the air composition. In addition, relatively lower coefficients of determination (R^2) were obtained in the open system than in the closed system. The coefficient of determination for all conditions in the closed system was close to one, which meant that the pseudo-zero-order reactions for the generation of H_2O_2 proceeded linearly due to their being no significant change in the dissolved gas content. As the dissolved gas content changed noticeably in the open system, the linearity of the H_2O_2 generation reaction decreased significantly. For the conditions in which the coefficient of determination was close to one in the open system, the negatively and positively affecting gas effect seemed to compensate for one another with no decrease in the linearity of the reactions during the 60 min irradiation, despite the drastic change in the dissolved gas content.

To further investigate the effect of gas exchange in the open system on the generation of H_2O_2, a gas saturation and re-saturation test was repeated twice for selected gas conditions including Ar 100 %, Ar:O_2 (75:25), Ar:O_2 (25:75), and O_2 100 % over a longer irradiation duration (90 min), as shown in Fig. 3. The H_2O_2 generation curve can be divided into two stages based on the linearity of the curve: the H_2O_2 concentration increased linearly during the first 45 min, and then increased linearly with a more gradual slope during the next 45 min. After gas re-saturation with the same gases, the decreasing slope for H_2O_2 generation recovered, and then the reduction of the slope occurred again at the same level. For several gas conditions, the pseudo-zero-order constants for the entire irradiation time (0–90 min), the first half of the irradiation time (0–45 min), and the second half of the irradiation time (45–90 min) are summarized with the coefficient of determination in Fig. 1S. The ratio of the constant for 45–90 min ($k_{45\text{-}90}$) to the constant for 0–45 min ($k_{0\text{-}45}$) was 0.82, 0.50, 0.58, 0.49, 0.63, 0.79, 1.15, and 1.11 for Ar 100 %, Ar:O_2 (75:25), Ar:O_2 (25:75), O_2 100 %, O_2:N_2 (75:25), O_2:N_2 (25:75), N_2 100 %, and N_2:Ar (25:75), respectively. The degree of H_2O_2 generation/accumulation decreased slightly after the gas content in the liquid changed significantly for most cases, except N_2 100 % and N_2:Ar (25:75). In addition, it was found that the conditions where the ratios of 0.5 to 0.6 were obtained showed relatively lower linearity in the open system (Fig. 2). The reason for the large difference between $k_{0\text{-}45}$ and $k_{45\text{-}90}$ in the Ar/O_2 mixture was the fast removal of positively affecting Ar and the entry of negatively affecting N_2, as discussed above. Considering the case of O_2 100 %, it was revealed again that an increase in the N_2 concentration in the liquid resulted in a remarkable decrease in the cavitational oxidizing activity. The ratio of $k_{45\text{-}90}$ to $k_{0\text{-}45}$ was greater than one for N_2 100 % and N_2:Ar (25:75) due to the dissolution of the positively affecting O_2 gas.

In the closed system of Ar:O_2 (75:25) or O_2:N_2 (25:75), the degradation of bisphenol A (BPA), which followed the pseudo-first-order reaction [57], was investigated briefly under the same experimental conditions. The initial BPA concentration was 10 mg/L. The pseudo first-order reaction constant was 1.76 ± 0.24 min^{-1} and 0.67 ± 0.00 min^{-1} for Ar:O_2 (75:25) or O_2:N_2 (25:75), respectively. The removal efficiencies after 240 min of irradiation were 35.1 % and 14.4 % for Ar:O_2 (75:25) and O_2:N_2 (25:75), respectively.

3.2. Gas sparging

The effect of gas sparging on cavitational H_2O_2 generation was investigated using the same gas conditions in closed and open systems, as shown in Fig. 4. The liquid was saturated and irradiated using ultrasound with continuous gas sparging for all cases. The initial gas content in the liquid was considered relatively constant in both the open and closed systems because the DO concentration did not change significantly owing to the continuous gas supply, as shown in Table 3. This resulted in similar reaction constants for open and closed systems under the same gas conditions. In addition, most coefficients of determination for both open and closed systems were close to one.

The application of gas sparging appeared to significantly enhance the cavitational oxidizing activity [4,14,21]. A much higher reaction constant for H_2O_2 generation was obtained under all the gas conditions. The enhancement ranged from 198 % (O_2 100 %) to 659 % [O_2:N_2 (25:75)] and from 241 % (O_2 100 %) to 719 % [O_2:N_2 (50:50)] for the closed and open systems, respectively. The highest constant was obtained for the Ar:O_2 (75:25) sparging condition in the closed system, as expected, and was four times greater than the highest constant in the gas saturation/closed condition of Ar:O_2 (75:25) (Fig. 2). The highest constant was obtained for the Ar:O_2 (75:25) sparging condition in the closed system (k_0 = 1 μM/min), as expected, and was four times greater than the highest constant in the gas saturation/closed condition of Ar:O_2 (75:25) (Fig. 2). Pflieger et al. reported the H_2O_2 generation rates of 12–27 μM/min under various gas sparging conditions (362 kHz, Ar:O_2 = 80:20, V_L = 0.25 L, P_{cal} = 73 W, Gas sparging rate: 20–130 mL/min) [14]. The large difference might be attributed to different experimental conditions including the frequency (28 kHz vs 362 kHz) and power density (15.1 W/L vs 292 W/L). In addition, the sparging of O_2:N_2 (25:75), similar to air, resulted in a kinetic constant as high as the highest constant in the gas saturation condition.

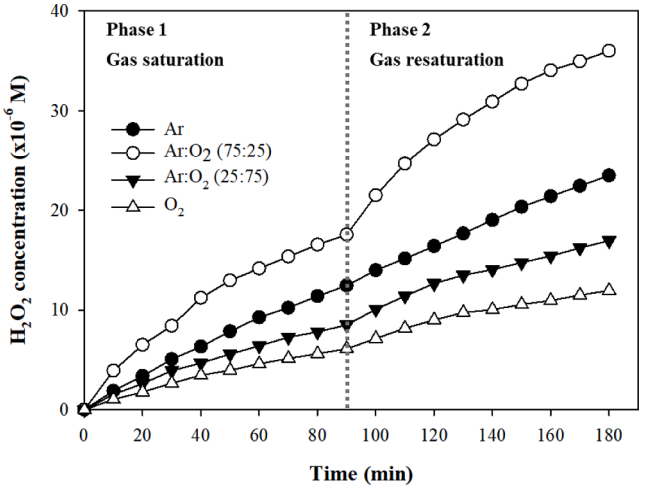

Fig. 3. Cavitational generation of H_2O_2 under various gas conditions. The gas saturation and re-saturation were repeated twice.

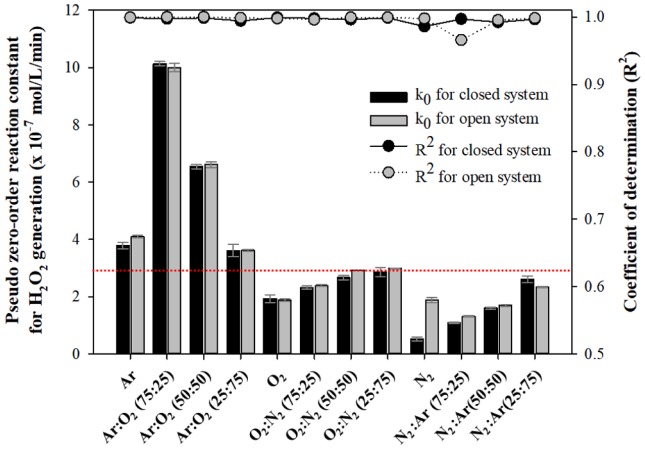

Fig. 4. Pseudo zero-order reaction constant and coefficient of determination for the 28 kHz cavitational generation of H_2O_2 under various gas sparging conditions in closed and open systems. The irradiation duration was 60 min and the gas sparging flow rate was 3 L/min. The red line represents the highest constant [Ar:O2 (75:25)] for the gas saturation conditions in Fig. 2.

Table 3
Variation of DO concentration before and after ultrasonic irradiation for various gas sparging conditions with a DO saturation concentration of 9.1 mg/L at 20 ℃.

Gas saturation		Ar	Ar:O_2 (75:25)	Ar:O_2 (50:50)	Ar:O_2 (25:75)	O_2	O_2:N_2 (75:25)	O_2:N_2 (50:50)	O_2:N_2 (25:75)	N_2	N_2:Ar (75:25)	N_2:Ar (50:50)	N_2:Ar (25:75)
Closed	DO_0* (mg/L)	0.2	10.2	21.0	30.4	39.5	30.8	20.8	10.8	0.5	0.2	0.2	0.3
	DO_{60}* (mg/L)	0.7	10.3	20.3	29.0	37.5	30.1	19.9	11.0	0.5	0.6	0.7	0.6
	ΔDO**	+0.5	+0.0	−0.7	−1.5	−2.0	−0.7	−0.9	+0.2	−0.0	+0.4	+0.5	+0.3
Open	DO_0 (mg/L)	0.2	10.8	20.7	30.3	39.8	29.2	19.8	10.2	0.7	0.2	0.2	0.2
	DO_{60} (mg/L)	0.8	11.0	20.0	28.9	38.0	29.0	19.0	10.0	1.9	0.6	0.5	0.5
	ΔDO	+0.5	+0.2	−0.8	−1.4	−1.8	−0.2	−0.8	−0.3	+1.2	+0.4	+0.3	+0.3

* DO_0 and DO_{60} represent DO concentrations before and after 60 min of irradiation, respectively.
** $\Delta DO = DO_{60}\text{-}DO_0$.

To visually understand the large enhancement induced by gas sparging, the SCL images were captured and analyzed for both gas saturation and gas sparging, as shown in Fig. 5. The cavitational reactions of luminol molecules and oxidizing radicals emit blue/white light. The bright area in the reactor is considered as a hot spot for oxidizing radical reactions, including H_2O_2 generation [28]. Because the SCL image represents 2-dimensional activity and there might be some distortions between the real active zone and the captured image, it was hard to obtain a proportional relationship between the H_2O_2 generation and the SCL intensity. However, the brightness, location, and area of light can be approximately related to the cavitational oxidizing activity in sonochemical reactors.

A brighter and larger area was observed in the SCL image for the Ar/O_2 mixture, where high reaction constants were obtained under both gas saturation and sparging conditions, as shown in Figs. 2 and 4. Conversely, less bright light, and a smaller area of light, was detected for the gas mixtures with N_2, and no noticeable light was observed for N_2 (100 %). The major differences in the SCL images between gas saturation and gas sparging were the location and shape of the active zone. For gas saturation conditions, the main active zone was observed in the standing wave field adjacent to the liquid surface [4,33,58,59]. As the liquid surface becomes more stable, a stronger and larger standing wave field is formed [4,33,60,61]. In this study, the liquid surface was stable under gas saturation conditions despite the generation of gentle ripples induced by ultrasonic irradiation. It should be noted that strong cavitational oxidizing activity was also observed in the region close to the bottom for Ar:O_2 (75:25) in the gas saturation condition. This may have been due to the presence of a gas mixture of Ar:O_2 (75:25), which was highly favorable for cavitational activity enhancement and enabled effective cavitation events to occur in a less strong ultrasonic energy field.

However, a bulb-shaped active zone was mainly observed in the region surrounding the gas sparger under gas sparging conditions. It appeared obvious that the bubble movement from the sparger significantly affected the formation of the bulb-shaped active zone, as shown in Fig. 5. The ultrasound transmission to the upper area was significantly inhibited by bubble clusters adjacent to the sparger and higher sonochemical oxidation activity was obtained as a result of the many gas molecules in the bottom region [4,21]. A weak and blurred standing wave field, which resulted from less ultrasonic transmission to the upper area and the unstable liquid surface with waves and ripples induced by the upstream bubbles, was also observed adjacent to the liquid surface for the gas conditions where less strong or low activity was detected. Notably, the standing wave field was rarely observed for gas conditions including Ar 100 % and Ar:O_2 mixtures, where relatively strong oxidizing activity was detected. This indicates that the degree of ultrasonic transmission through the bubble clusters may vary significantly depending on the gas composition of the bubbles.

To investigate the effect of the gas content on the sound energy level, the sound energy level was measured using a hydrophone and spectrum analyzer for Ar:O_2 (75:25) and N_2:O_2 (75:25). The sparger was placed at the bottom of the reactor and the hydrophone was placed at the middle height of the liquid above the bubble clusters generated from the sparger. As shown in Fig. 2S, no significant difference was observed between the two conditions. However, it should be noted that clearer and higher peaks of harmonic frequencies (2f, 3f, 4f, •••) and less clear and lower peaks of sub-harmonics (1.5f, 2.5f, 3.5f, •••) in the frequency range of 0–200 kHz were observed for Ar:O_2 (75:25) than for N_2:O2 (75:25) [62]. The effect of the gas sparging rate was also investigated, as shown in Fig. 3S. The sound pressure level decreased significantly for Ar:O_2 (75:25) as the gas flow rate increased from 0 L/min to 10 L/min, as shown in Fig. S3. Therefore, ultrasonic blockage by gas sparging occurred, resulting in the formation of a concentrated active zone adjacent to the sparger at the bottom area. The effect of the sparging rate on H_2O_2 generation is discussed in Section 3.3.

The reasons for the enhancement of the H_2O_2 generation by the gas

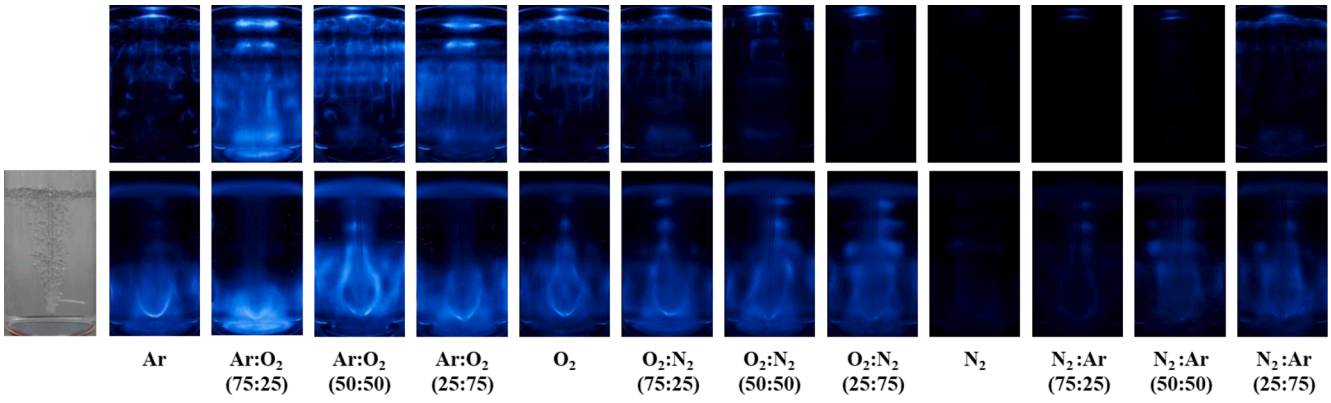

Fig. 5. Real and SCL images under various gas mixtures for gas saturation and sparging conditions. The gas sparging flow rate was 3 L/min.

sparging can be explained as follows: Firstly, the positively affecting gas molecules (Ar or O_2) were provided continuously, inducing the immediate removal of negatively affecting gas molecules (N_2), which might have entered due to the concentration gradient between the liquid and the air, for the Ar or O_2 sparging/open conditions. Secondly, gas sparging can induce violent mixing, as in bubble column reactors, which leads to the active movement of reactants in the reactor. Thirdly, the formation of bubble clusters adjacent to the sparger significantly altered the shape and location of the cavitational active zone, as shown in the SCL images in Fig. 5. The bubble clusters surrounding the sparger acted as unstable and continuously transforming reflectors, and a highly active zone formed under the bubble clusters. It was reported that mechanical mixing in the liquid phase resulted in similar changes in the cavitational active zone [5]. Fourth, the gas molecules, which were supplied continuously, acted as nuclei for cavitation, inducing more cavitation and radicals.

3.3. Gas sparging rate and sparger position

The effects of the sparging gas flow rate and sparger position on the generation of H_2O_2 were investigated for Ar:O_2 (75:25), as shown in Fig. 6. The SCL images are shown in Fig. 7. As the gas flow rate increased, the reaction constant increased significantly and then remained relatively constant [4,14]. For the lower flow rate conditions, the sonochemical reactions occurred in both the lower zone adjacent to the sparger and the upper zone. The highest constant was obtained for 3 L/min. No standing wave field was observed for rates higher than 3 L/min, which was attributed to the ultrasonic energy trapping by bubble clouds and the formation of an unstable liquid surface, as discussed in Section 3.2. The gradual disappearance of the standing wave field in the upper area and the gradual increase in the instability of the liquid surface are shown in Fig. 7. No significant enhancements were observed at 5 L/min and 10 L/min. This might be due to the generation of much larger bubbles from the sparger, which was effective in trapping the ultrasound and ineffective in terms of dissolution of gas molecules from the bubbles into the liquid. The minor change between 3 L/min and 10 L/min might also have been due to the compensating effects of the decrease in the sound pressure levels, as shown in Fig. 3S, and the enhanced mixing intensity in the liquid.

Gas sparging at the bottom resulted in the highest cavitation activity [4]. When the sparger was placed at the middle or top position, the formation of a standing wave field was observed, and noticeably lower cavitational activity was obtained. This was attributed to less blockage

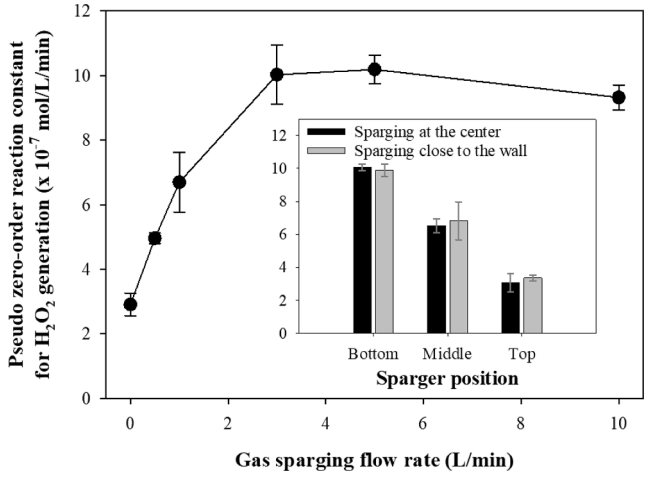

Fig. 6. Pseudo zero-order reaction constant for the 28 kHz cavitational generation of H_2O_2 under various gas sparging flow rates. The inset represents the pseudo zero-order reaction constant for various sparger positions. The sparging gas was Ar:O_2 (75:25).

of ultrasonic transmission to the upper zone and a less unstable liquid surface. Therefore, it was found that upward ultrasonic transmission was significantly affected by the formation of bubble clusters adjacent to the sound source, as shown in the SCL images of Fig. 7.

No significant difference was observed between sparging at the center and close to the wall. In our previous study using larger rectangular sonoreactors (4.5–15.5 L), the gas sparging at the center of the transducer module at the bottom induced higher cavitational activity than did the sparging at the corner of the transducer because the sparing at the corner could not block the ultrasonic transmission effectively owing to the larger area of the transducer compared to the size of the bubble cluster [4]. Pflieger et al. reported that the slope of H_2O_2 generation changed significantly when the sparger position was moved [19]. In this study, it appeared that the degree of suppression for the ultrasonic irradiation was quite similar for both sparging at the center and close to the wall, even though quite different SCL images were obtained for each scenario. This might be due to the relatively small area of the reactor and transducer used in this study, considering the effective area of the gas sparging.

Consequently, the gas sparging position could affect the degree of sonochemical activity because the cavitational active zone changed significantly owing to the variation in the sound pressure levels. There might be an optimal sparging position and gas flow rate for the enhancement of sonochemical activity, considering the characteristics of sonoreactors, including liquid height and volume. The highest sonochemical activity was obtained when the sparging of 3 L/min was applied adjacent to the ultrasonic source.

4. Conclusion

The effects of gas saturation and sparging on sonochemical oxidation activity and the generation of H_2O_2 were investigated using a 28 kHz sonoreactor equipped with a gas supply system in this study (part I). Twelve gas conditions including Ar 100 %, O_2 100 %, N_2 100 %, and binary gas mixtures, were applied under four gas modes: saturation/closed, saturation/open, sparging/closed, and sparging/open. The formation of the sonochemical active zone was visually analyzed using the SCL method. The conclusions of this study are as follows:

1. The saturation gas composition in the liquid phase significantly affected the sonochemical oxidation activity. A mixture of Ar/O_2 (75:25 or 50:50) resulted in the highest H_2O_2 generation, and the presence of N_2 undermined the activity. The gas content changed significantly in the saturation/open mode, and the DO concentration can be used as an indicator of the change in the saturation gas content.
2. Gas sparging remarkably enhanced the sonochemical oxidation activity, which was attributed to the variation of the cavitational active zone in terms of location, shape, and intensity. Without gas sparging, the standing wave field adjacent to the liquid surface was the main active zone. In contrast, a hot spot formed close to the sparger at the bottom when sparging was applied.
3. The sparging gas flow rate and sparger location also noticeably affected the sonochemical oxidation activity. The change in the sonochemical oxidation activity was mainly related to the characteristics of the bubbles from the sparger, the resulting change in the ultrasonic energy distribution, and the corresponding sonochemical active zone.

CRediT authorship contribution statement

Younggyu Son: Conceptualization, Methodology, Writing – original draft, Writing – review & editing, Visualization, Supervision, Funding acquisition. **Jieun Seo:** Methodology, Investigation, Validation.

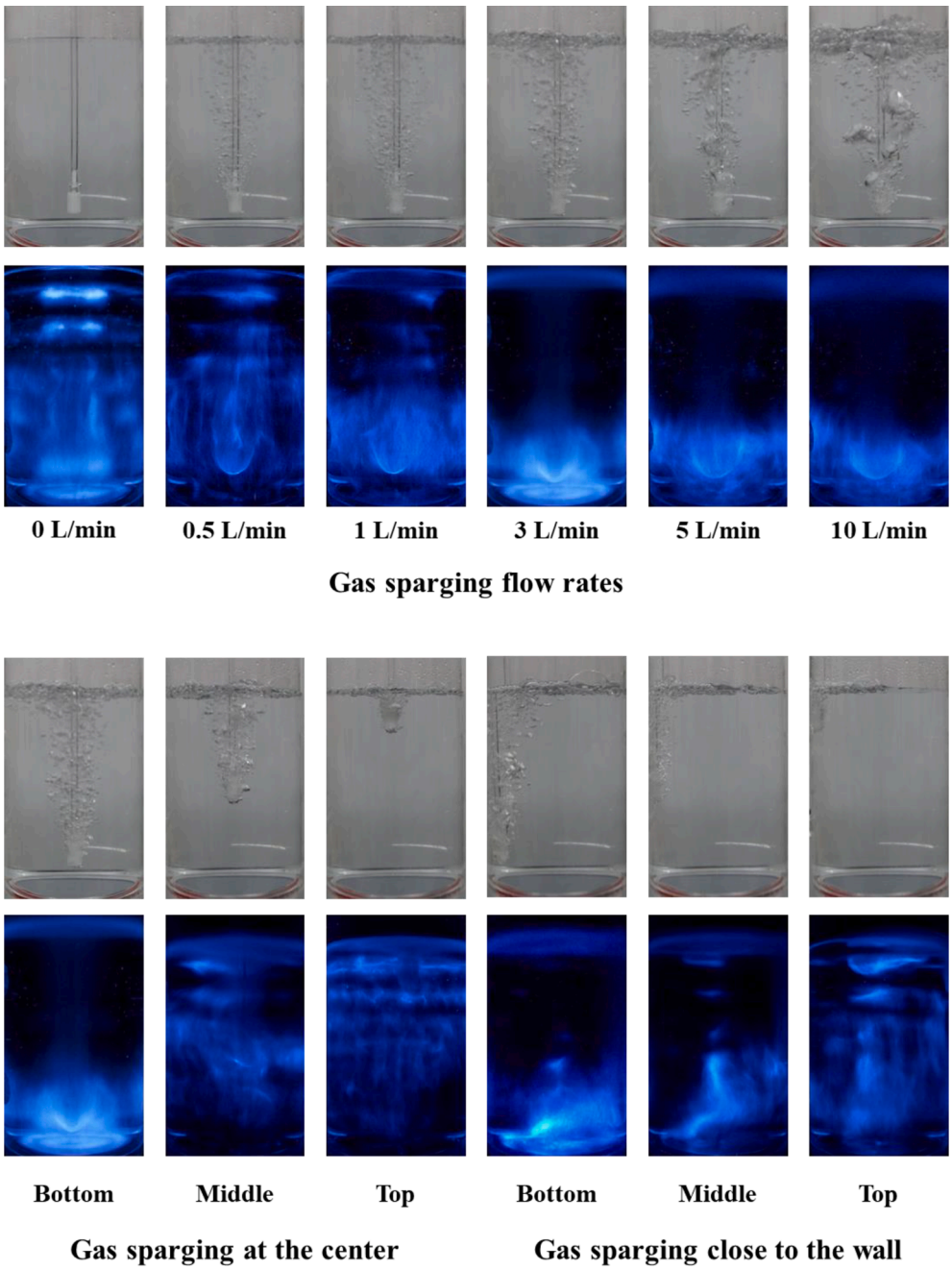

Fig. 7. Real and SCL images under various gas flow rates and gas sparging positions. The sparging gas was Ar:O2 (75:25).

Declaration of Competing Interest

The authors declare that they have no known competing financial interests or personal relationships that could have appeared to influence the work reported in this paper.

Data availability

No data was used for the research described in the article.

Acknowledgments

This work was supported by the National Research Foundation of Korea [NRF-2021R1A2C1005470] and by the Korea Ministry of Environment (MOE) as "Subsurface Environment Management (SEM)" Program [project No. 2021002470001].

Appendix A. Supplementary data

Supplementary data to this article can be found online at https://doi.org/10.1016/j.ultsonch.2022.106214.

References

[1] J. Rooze, E.V. Rebrov, J.C. Schouten, J.T.F. Keurentjes, Dissolved gas and ultrasonic cavitation – A review, Ultrason. Sonochem. 20 (1) (2013) 1–11.
[2] R.J. Wood, J. Lee, M.J. Bussemaker, A parametric review of sonochemistry: Control and augmentation of sonochemical activity in aqueous solutions, Ultrason. Sonochem. 38 (2017) 351–370.
[3] Y. Ono, K. Shinashi, H. Tanaka, H. Harada, Mechanism of improving the rate of sono-oxidation of a KI solution by introduction of CO_2 into an Ar atmosphere, Ultrason. Sonochem. 51 (2019) 145–150.
[4] J. Choi, J. Khim, B. Neppolian, Y. Son, Enhancement of sonochemical oxidation reactions using air sparging in a 36 kHz sonoreactor, Ultrason. Sonochem. 51 (2019) 412–418.

[5] J. Choi, H. Lee, Y. Son, Effects of gas sparging and mechanical mixing on sonochemical oxidation activity, Ultrason. Sonochem. 70 (2021), 105334.
[6] G. Mark, A. Tauber, R. Laupert, H.-P. Schuchmann, D. Schulz, A. Mues, C. von Sonntag, OH-radical formation by ultrasound in aqueous solution – Part II: Terephthalate and Fricke dosimetry and the influence of various conditions on the sonolytic yield, Ultrason. Sonochem. 5 (1998) 41–52.
[7] I. Hua, M.R. Hoffmann, Optimization of ultrasonic irradiation as an advanced oxidation technology, Environ. Sci. Technol. 31 (8) (1997) 2237–2243.
[8] M.A. Beckett, I. Hua, Impact of ultrasonic frequency on aqueous sonoluminescence and sonochemistry, J. Phys. Chem. A 105 (15) (2001) 3796–3802.
[9] C.H. Fischer, E.J. Hart, A. Henglein, Ultrasonic irradiation of water in the presence of oxygen 18,18O_2: isotope exchange and isotopic distribution of hydrogen peroxide, J. Phys. Chem. 90 (1986) 1954–1956.
[10] S. Merouani, H. Ferkous, O. Hamdaoui, Y. Rezgui, M. Guemini, New interpretation of the effects of argon-saturating gas toward sonochemical reactions, Ultrason. Sonochem. 23 (2015) 37–45.
[11] U.W. Weber, P.G. Cook, M.S. Brennwald, R. Kipfer, T.C. Stieglitz, A novel approach to quantify air-water gas exchange in shallow surface waters using high-resolution time series of dissolved atmospheric gases, Environ. Sci. Technol. 53 (3) (2019) 1463–1470.
[12] H. Yanagida, The effect of dissolve gas concentration in the initial growth stage of multi cavitation bubbles: Differences between vacuum degassing and ultrasound degassing, Ultrason. Sonochem. 15 (2008) 492–496.
[13] N. Gondrexon, V. Renaudin, P. Boldo, Y. Gonthier, A. Bernis, C. Pettier, Degassing effect and gas-liquid transfer in a high frequency sonochemical reactor, Chem. Eng. J. 66 (1) (1997) 21–26.
[14] R. Pflieger, T. Chave, G. Vite, L. Jouve, S.I. Nikitenko, Effect of operational conditions on sonoluminescence and kinetics of H_2O_2 formation during the sonolysis of water in the presence of Ar/O_2 gas mixture, Ultrason. Sonochem. 26 (2015) 169–175.
[15] J.M. Meichtry, L. Cancelada, H. Destaillats, M.I. Litter, Effect of different gases on the sonochemical Cr(VI) reduction in the presence of citric acid, Chemosphere 260 (2020), 127211.
[16] L.M. Kwedi-Nsah, T. Kobayashi, Sonochemical nitrogen fixation for the generation of NO_2^- and NO_3^- ions under high-powered ultrasound in aqueous medium, Ultrason. Sonochem. 66 (2020), 105051.
[17] J.D. Schramm, I. Hua, Ultrasonic irradiation of dichlorvos: decomposition mechanism, Water Res. 35 (3) (2001) 665–674.
[18] H. Ferkous, O. Hamdaoui, S. Merouani, Sonochemical degradation of naphthol blue black in water: Effect of operating parameters, Ultrason. Sonochem. 26 (2015) 40–47.
[19] R. Pflieger, L. Gravier, G. Guillot, M. Ashokkumar, S.I. Nikitenko, Inverse effects of the gas feed positioning on sonochemistry and sonoluminescence, Ultrason. Sonochem. 46 (2018) 10–17.
[20] J. Rooze, E.V. Rebrov, J.C. Schouten, J.T.F. Keurentjes, Effect of resonance frequency, power input, and saturation gas type on the oxidation efficiency of an ultrasound horn, Ultrason. Sonochem. 18 (1) (2011) 209–215.
[21] T. Tuziuti, K. Yasui, T. Kozuka, A. Towata, Y. Iida, Enhancement of sonochemical reaction rate by addition of micrometer-sized air bubbles, J. Phys. Chem. A 110 (37) (2006) 10720–10724.
[22] L. Pi, J. Cai, L. Xiong, J. Cui, H. Hua, D. Tang, X. Mao, Generation of H_2O_2 by on-site activation of molecular dioxygen for environmental remediation applications: A review, Chem. Eng. J. 389 (2020), 123420.
[23] J. Liu, Y. Zou, B. Jin, K. Zhang, J.H. Park, Hydrogen Peroxide Production from Solar Water Oxidation, ACS Energy Lett. 4 (12) (2019) 3018–3027.
[24] C. Petrier, A. Jeunet, J.L. Luche, G. Reverdy, Unexpected frequency effects on the rate of oxidative processes induced by ultrasound, J. Am. Chem. Soc. 114 (8) (1992) 3148–3150.
[25] S.I. Nikitenko, C. Le Naour, P. Moisy, Comparative study of sonochemical reactors with different geometry using thermal and chemical probes, Ultrason. Sonochem. 14 (3) (2007) 330–336.
[26] E. Dalodière, M. Virot, P. Moisy, S.I. Nikitenko, Effect of ultrasonic frequency on H_2O_2 sonochemical formation rate in aqueous nitric acid solutions in the presence of oxygen, Ultrason. Sonochem. 29 (2016) 198–204.
[27] R. Ji, R. Pflieger, M. Virot, S.I. Nikitenko, Multibubble sonochemistry and sonoluminescence at 100 kHz: the missing link between low- and high-frequency ultrasound, J. Phys. Chem. B 122 (2018) 6989–6994.
[28] Y. Son, Simple design strategy for bath-type high-frequency sonoreactors, Chem. Eng. J. 328 (2017) 654–664.
[29] Y. Son, M. Lim, J. Khim, M. Ashokkumar, Attenuation of UV light in large-scale sonophotocatalytic reactors: the effects of ultrasound irradiation and TiO_2 concentration, Ind. Eng. Chem. Res. 51 (2012) 232–239.
[30] Y. Son, M. Lim, J. Khim, Investigation of acoustic cavitation energy in a large-scale sonoreactor, Ultrason. Sonochem. 16 (4) (2009) 552–556.
[31] Y. Asakura, T. Nishida, T. Matsuoka, S. Koda, Effects of ultrasonic frequency and liquid height on sonochemical efficiency of large-scale sonochemical reactors, Ultrason. Sonochem. 15 (3) (2008) 244–250.
[32] Y. Son, M. Lim, J. Song, J. Khim, Liquid height effect on sonochemical reactions in a 35 kHz sonoreactor, Jpn. J. Appl. Phys. 48 (2009) 07GM16.
[33] Y. Son, M. Lim, M. Ashokkumar, J. Khim, Geometric Optimization of Sonoreactors for the Enhancement of Sonochemical Activity, J. Phys. Chem. C 115 (10) (2011) 4096–4103.
[34] D. Lee, Y. Son, Ultrasound-assisted soil washing processes using organic solvents for the remediation of PCBs-contaminated soils, Ultrason. Sonochem. 80 (2021) 105825.
[35] M. Lim, M. Ashokkumar, Y. Son, The effects of liquid height/volume, initial concentration of reactant and acoustic power on sonochemical oxidation, Ultrason. Sonochem. 21 (6) (2014) 1988–1993.
[36] Y. Son, Y. No, J. Kim, Geometric and operational optimization of 20-kHz probe-type sonoreactor for enhancing sonochemical activity, Ultrason. Sonochem. 65 (2020), 105065.
[37] D. Lee, I. Na, Y. Son, Effect of liquid recirculation flow on sonochemical oxidation activity in a 28 kHz sonoreactor, Chemosphere 286 (2022), 131780.
[38] J. Choi, Y. Son, Quantification of sonochemical and sonophysical effects in a 20 kHz probe-type sonoreactor: Enhancing sonophysical effects in heterogeneous systems with milli-sized particles, Ultrason. Sonochem. 82 (2022), 105888.
[39] S. Merouani, O. Hamdaoui, Y. Rezgui, M. Guemini, Sensitivity of free radicals production in acoustically driven bubble to the ultrasonic frequency and nature of dissolved gases, Ultrason. Sonochem. 22 (2015) 41–50.
[40] R. Chauhan, G.K. Dinesh, B. Alawa, S. Chakma, A critical analysis of sono-hybrid advanced oxidation process of ferrioxalate system for degradation of recalcitrant pollutants, Chemosphere 277 (2021), 130324.
[41] N. Her, J.-S. Park, Y. Yoon, Sonochemical enhancement of hydrogen peroxide production by inert glass beads and TiO_2-coated glass beads in water, Chem. Eng. J. 166 (1) (2011) 184–190.
[42] S. Merouani, O. Hamdaoui, F. Saoudi, M. Chiha, Influence of experimental parameters on sonochemistry dosimetries: KI oxidation, Fricke reaction and H_2O_2 production, J. Hazard. Mater. 178 (2010) 1007–1014.
[43] M. Inoue, F. Okada, A. Sakurai, M. Sakakibara, A new development of dyestuffs degradation system using ultrasound, Ultrason. Sonochem. 13 (4) (2006) 313–320.
[44] Y. Kojima, T. Fujita, E.P. Ona, H. Matsuda, S. Koda, N. Tanahashi, Y. Asakura, Effects of dissolved gas species on ultrasonic degradation of (4-chloro-2-methylphenoxy) acetic acid (MCPA) in aqueous solution, Ultrason. Sonochem. 12 (5) (2005) 359–365.
[45] J.-J. Yao, N.-Y. Gao, Y. Deng, Y. Ma, H.-J. Li, B. Xu, L. Li, Sonolytic degradation of parathion and the formation of byproducts, Ultrason. Sonochem. 17 (5) (2010) 802–809.
[46] Y. Mizukoshi, T. Shuto, N. Masahashi, S. Tanabe, Preparation of superparamagnetic magnetite nanoparticles by reverse precipitation method: Contribution of sonochemically generated oxidants, Ultrason. Sonochem. 16 (4) (2009) 525–531.
[47] B. Gielen, S. Marchal, J. Jordens, L.C.J. Thomassen, L. Braeken, T. Van Gerven, Influence of dissolved gases on sonochemistry and sonoluminescence in a flow reactor, Ultrason. Sonochem. 31 (2016) 463–472.
[48] K. Yasui, T. Tuziuti, Y. Iida, H. Mitome, Theoretical study of the ambient-pressure dependence of sonochemical reactions, J. Chem. Phys. 119 (1) (2003) 346–356.
[49] K. Yasui, T. Tuziuti, T. Kozuka, A. Towata, Y. Iida, Relationship between the bubble temperature and main oxidant created inside an air bubble under ultrasound, J. Chem. Phys. 127 (2007), 154502.
[50] K. Okitsu, T. Suzuki, N. Takenaka, H. Bandow, R. Nishimura, Y. Maeda, Acoustic multibubble cavitation in water: a new aspect of the effect of a rare gas atmosphere on bubble temperature and its relevance to sonochemistry, J. Phys. Chem. B 110 (2006) 20081–20084.
[51] Y. Iida, M. Ashokkumar, T. Tuziuti, T. Kozuka, K. Yasui, A. Towata, J. Lee, Bubble population phenomena in sonochemical reactor: II. Estimation of bubble size distribution and its number density by simple coalescence model calculation, Ultrason. Sonochem. 17 (2010) 480–486.
[52] B.-K. Kang, M.-S. Kim, J.-G. Park, Effect of dissolved gases in water on acoustic cavitation and bubble growth rate in 0.83MHz megasonic of interest to wafer cleaning, Ultrason. Sonochem. 21 (4) (2014) 1496–1503.
[53] W.M. Haynes, D.R. Lide, T.J. Bruno, CRC handbook of chemistry and physics: a ready-reference book of chemical and physical data. 2016–2017, 97th ed., CRC Press, Florida, 2016.
[54] C. Pétrier, E. Combet, T. Mason, Oxygen-induced concurrent ultrasonic degradation of volatile and non-volatile aromatic compounds, Ultrason. Sonochem. 14 (2) (2007) 117–121.
[55] B. Li, Y. Gu, M. Chen, An experimental study on the cavitation of water with dissolved gases, Exp. Fluids 58 (2017) 164.
[56] Y. Asakura, K. Yasuda, Frequency and power dependence of ultrasonic degassing, Ultrason. Sonochem. 82 (2022) 105890.
[57] R.A. Torres, C. Pétrier, E. Combet, M. Carrier, C. Pulgarin, Ultrasonic cavitation applied to the treatment of bisphenol A. Effect of sonochemical parameters and analysis of BPA by-products, Ultrason. Sonochem. 15 (4) (2008) 605–611.
[58] M. Ashokkumar, J. Lee, Y. Iida, K. Yasui, T. Kozuka, T. Tuziuti, A. Towata, The detection and control of stable and transient acoustic cavitation bubbles, Phys. Chem. Chem. Phys. 11 (2009) 10118–10121.
[59] S. Saito, Chapter 2 – ultrasound field and bubbles, in: F. Grieser, P.K. Choi, N. Enomoto, H. Harada, K. Okitsu, K. Yasui (Eds.), Sonochemistry and the Acoustic Bubble, Elsevier, Amsterdam, 2015, pp. 11–39.
[60] J. Lee, K. Yasui, T. Tuziuti, T. Kozuka, A. Towata, Y. Iida, Spatial distribution enhancement of sonoluminescence activity by altering sonication and solution conditions, J. Phys. Chem. B 112 (48) (2008) 15333–15341.
[61] T. Tuziuti, K. Yasui, T. Kozuka, A. Towata, Y. Iida, Suppression of sonochemiluminescence reduction at high acoustic amplitudes by the addition of particles, J. Phys. Chem. A 111 (48) (2007) 12093–12098.
[62] Y. Son, M. Lim, J. Khim, M. Ashokkumar, Acoustic emission spectra and sonochemical activity in a 36 kHz sonoreactor, Ultrason. Sonochem. 19 (2012) 16–21.